

Chaos and threshold for irreversibility in sheared suspensions

D. J. Pine^{1,2}, J. P. Gollub^{1,3}, J. F. Brady⁴ & A. M. Leshansky⁵

Systems governed by time reversible equations of motion often give rise to irreversible behaviour^{1–3}. The transition from reversible to irreversible behaviour is fundamental to statistical physics, but has not been observed experimentally in many-body systems. The flow of a newtonian fluid at low Reynolds number can be reversible: for example, if the fluid between concentric cylinders is sheared by boundary motion that is subsequently reversed, then all fluid elements return to their starting positions⁴. Similarly, slowly sheared suspensions of solid particles, which occur widely in nature and science⁵, are governed by time reversible equations of motion. Here we report an experiment showing precisely how time reversibility⁶ fails for slowly sheared suspensions. We find that there is a concentration dependent threshold for the deformation or strain beyond which particles do not return to their starting configurations after one or more cycles. Instead, their displacements follow the statistics of an anisotropic random walk⁷. By comparing the experimental results with numerical simulations, we demonstrate that the threshold strain is associated with a pronounced growth in the Lyapunov exponent (a measure of the strength of chaotic particle interactions). The comparison illuminates the connections between chaos, reversibility and predictability.

The time reversibility of simple shear flows at low Reynolds number (Re) is demonstrated in a film by Taylor⁸. A drop of dye is placed in a fluid in the gap between concentric cylinders (a configuration known as circular Couette flow) and the inner cylinder rotated many turns. The drop seems to disappear as it spreads into a thin filament, but is reconstituted almost without change (except for slight blurring due to brownian motion) when the rotation is reversed. This behaviour is consistent with the time reversibility of the dynamical equations—the Stokes or ‘creeping flow’ equations⁴—that govern low Re flow. The same is not true for three-dimensional steady flows, which can exhibit chaotic advection and irreversibility⁹.

The reversible creeping flow equations also govern the low Re behaviour of a suspension of non-brownian particles (that is, particles too large to exhibit significant thermal motion). However, it was recently shown that in the creeping flow limit, the particle trajectories are chaotic¹⁰: that is, the suspended particles exhibit sensitive dependence on their initial (or current) positions. When the particle motion is described in a configuration space spanned by the $3N$ particle coordinates, nearby trajectories (in phase space) separate exponentially in time at a rate given by a positive Lyapunov exponent, λ . An earlier numerical study of only three particles falling through a viscous fluid also reveals chaotic particle dynamics¹¹. Thus, chaos is an intrinsic property of low Re flow of non-brownian suspensions.

In chaotic dynamical systems, trajectories are extremely sensitive to small perturbations from the deterministic paths dictated by

the dynamical equations. Since small perturbations are inevitably present, chaos may make it impossible for the system to retrace its microscopic dynamical path when reversed. Equivalently, chaos plus perturbations (noise) may lead to a loss of predictability after a finite time horizon¹². Normally, these properties are inferred from numerical solutions, since it is generally not possible to reconstitute the initial conditions in a real experiment, slightly perturb the system, and then follow its subsequent evolution. For a low Re non-brownian suspension, however, reversing the boundary motion is equivalent to reversing time. Thus, we have a unique opportunity to test the limits of reversibility and predictability experimentally: we can undertake a quantitative version of Taylor’s experiment and measure the degree to which particles return to their initial positions.

Previous experimental^{13–17} and numerical^{18,19} investigations show that the trajectories of non-brownian particles exhibit irregular and apparently random displacements, or effective diffusion, when a suspension is sheared unidirectionally between concentric cylinders with the inner one rotating (circular Couette flow). The origin of this irregular motion lies in the interactions between particles mediated by the fluid. Such interactions have been shown to produce a variety of important effects in suspensions, strongly affecting sedimentation^{20,21}, and causing particles to cluster²². However, the question of whether or not particle trajectories are reversible in one-dimensional shear flows has not been addressed experimentally.

Here we report a study of reversibility, which is made by straining a viscous suspension periodically in circular Couette flow. The time dependence of the strain γ , defined as the ratio of the azimuthal displacement of the inner cylinder to the width of the gap between the cylinders, is given by $\gamma(t) = \gamma_0 \sin \omega t$, where ω is the angular frequency of flow reversals and t is the time. The strain amplitude γ_0 is typically in the range 0.5–12. Straining the system to strain amplitude γ_0 evolves the system forward in time; by reversing the flow in the next quarter cycle, we can check to see if the particles return to their initial positions. Repeated sampling over many periods constitutes a severe test of reversibility, and allows the behaviour to be characterized statistically.

The suspension is composed of spherical polymethylmethacrylate (PMMA) particles of diameter $d = 230 \pm 20 \mu\text{m}$ dispersed in a multi-component fluid at a volume fraction ϕ in the range 0.1–0.4. The concentrations of the fluid components are adjusted²³ to match the density of the spheres (to avoid settling) and refractive index (to make the suspension transparent). A small number of particles are dyed black so that their positions can be tracked. The period of rotation is 5–100 s, and Re, based on the gap and the maximum fluid velocity, is held fixed at 0.001. Therefore, the low Re description applies.

Once oscillatory shear flow is established, the suspension is illuminated and the positions of the dyed particles recorded once

¹Department of Chemical Engineering and KITP, University of California, Santa Barbara, California 93106-5080, USA. ²Department of Physics and Center for Soft Matter Research, New York University, 2-4 Washington Place, New York, New York 10003, USA. ³Department of Physics, Haverford College, Haverford, Pennsylvania 19041, USA.

⁴Division of Chemistry and Chemical Engineering, California Institute of Technology, Pasadena, California 91125, USA. ⁵Department of Chemical Engineering, Technion - Israel Institute of Technology, Haifa 32000, Israel.

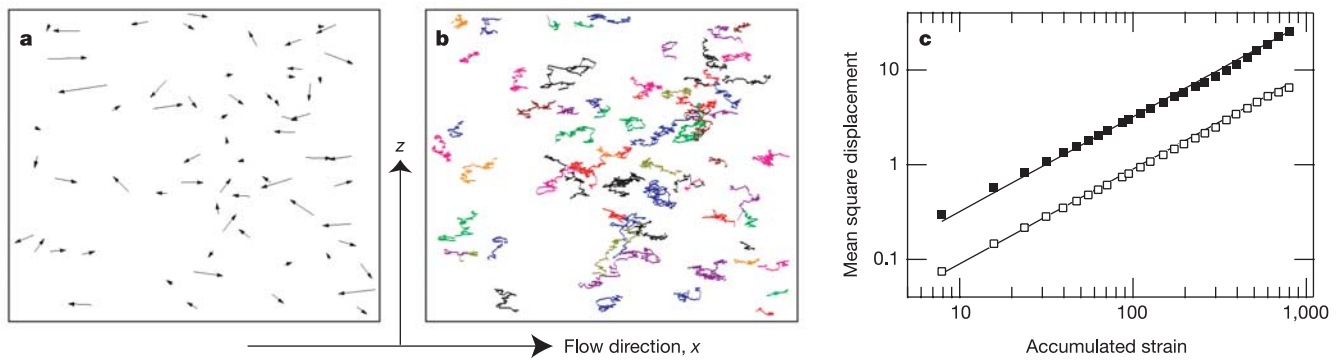


Figure 1 | Particle displacements and trajectories. **a**, Particle displacements in the x - z plane after one full cycle in a sheared suspension above the onset of irreversibility, amplified by a factor of 6 for clarity (volume fraction $\phi = 0.30$, strain amplitude $\gamma_0 = 2$). **b**, Some of the chaotic particle trajectories. **c**, Mean square particle displacements $\langle \Delta x^2 \rangle$ and $\langle \Delta z^2 \rangle$ after n full cycles as a function of the accumulated strain $\gamma = 4\gamma_0 n$ for $\phi = 0.40$ and $\gamma = 2.0$. The filled and open squares are the mean square displacements $\langle x^2 \rangle$ and $\langle z^2 \rangle$, respectively, obtained by averaging over particle trajectories such as those displayed in **b**; the solid lines through the data are least squares fits from which the diffusivities are determined. The fluctuations are anisotropic, growing more quickly along the flow direction (x) than along the axial direction (z). Experimental details: the diameter of the inner

cylinder of the Couette cell is 50 mm and the gap between the (concentric) cylinders is 2.5 mm; thus, a strain of 1 corresponds to an angular displacement of the inner cylinder of 5.7° . The PMMA particles have surface irregularities of only 2 nm, as measured by AFM. The fluid viscosity is 3 Pa s, about 3,000 times that of water. The suspension floats on a layer of mercury to eliminate end effects. The fractional accuracy of the phase at which the camera and frame grabber are triggered is typically better than 0.001, but the final results are not very sensitive to this quantity. We sample particle positions near the instant of maximum particle velocity. The particle displacements in the x and z directions after each full cycle are denoted by Δx and Δz , respectively.

per cycle using a camera and frame grabber. The total accumulated strain experienced by the particles over a run (taken to be positive at each instant) is $\gamma \equiv 4\gamma_0 n$, where n is the number of cycles, because the strain is γ_0 in each quarter cycle. To study the particle motion, we use tracking software²⁴ to locate the dark particles, whose coordinates x (along the direction of rotation) and z (along the cylinder axis) are tracked over the duration of the run. Sometimes particles are lost from view, but we typically track 60 particles or more over a total strain of 1,000 or so. This is ample to produce statistically accurate results.

We begin by describing the behaviour of the 30% concentration sample ($\phi = 0.30$). When γ_0 is less than about 1, all particles return to their original positions after each full cycle. On the other hand, if $\gamma_0 = 2$, the tracer particles fail to return by irregular amounts of typical magnitude $0.6d$ each cycle. These displacements are shown in Fig. 1a, and are larger along the flow (x) direction than along the axial (z) direction. The irreversibility after a full cycle, while comparable to the particle diameter, is substantially less than the typical displacement within a cycle. Trajectories sampled over many complete periods are shown in Fig. 1b; movies of both continuously and periodically sampled motion may be found in the Supplementary Information.

A statistical analysis of the motion, shown in Fig. 1c for $\phi = 0.40$, shows that the mean square particle displacements $\langle \Delta x^2 \rangle$ and $\langle \Delta z^2 \rangle$ after an integral number of cycles, averaged over many particles, are linear in the accumulated strain. The mean square displacements are also linear in time for a given driving frequency and strain amplitude, but what counts is the total strain. Data are essentially identical if Re is increased by a factor of 5; this shows that residual effects of the fluid inertia are not important. The anisotropy of shear flow leads to different magnitudes for $\langle \Delta x^2 \rangle$ and $\langle \Delta z^2 \rangle$. Anisotropy in particle transport also occurs for steady shearing, and is a consequence of ‘Taylor dispersion’²⁵.

We use these graphs of the mean square displacements to define non-dimensional effective diffusivities D_x and D_z along x and z , respectively, in the conventional way, but with total accumulated strain replacing time:

$$\langle (\Delta x/d)^2 \rangle = 2D_x \gamma \quad (1)$$

Equation (1) defines a dimensionless diffusivity that is independent

of the oscillation frequency, as we check empirically, thus allowing diffusivities measured at different frequencies and strain amplitudes to be compared meaningfully. Since the only natural time and length scales (other than the container dimensions) are the r.m.s. strain rate $\dot{\gamma}_{\text{rms}}$ and the particle diameter d , the dimensional particle diffusivity

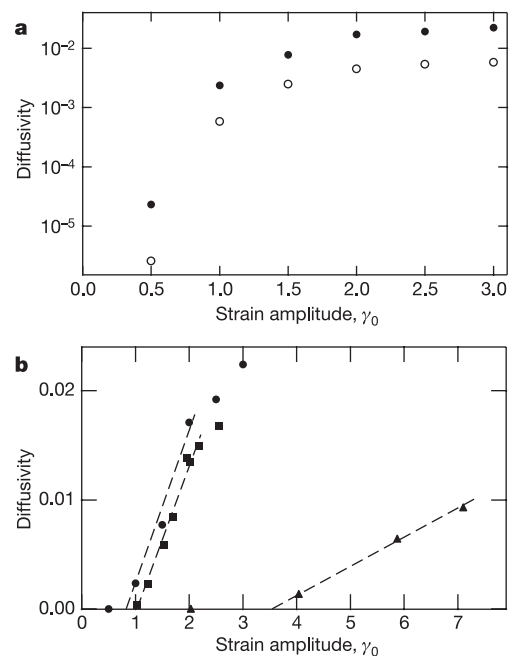


Figure 2 | Experimental diffusivities. **a**, Experimental effective diffusivities D_x (filled circles) and D_z (open circles) as a function of the oscillatory strain amplitude, on a logarithmic scale for volume fraction $\phi = 0.40$. The x and z diffusivities both become negligible for $\gamma_0 < 1$. **b**, Diffusivities D_x on a linear scale for three samples at different particle concentrations with linear extrapolations to zero diffusivity: triangles, $\phi = 0.20$; squares, $\phi = 0.30$; circles, $\phi = 0.40$. Data for D_z are omitted for clarity but extrapolate to the same values of the strain amplitude thresholds for the different concentrations.

D'_x defined by the dimensional form of equation (1), $\langle \Delta x^2 \rangle = 2D'_x t$, must scale like $D'_x \sim d^2 \dot{\gamma}_{\text{rms}}$.

The variation of the dimensionless diffusivities with strain amplitude for the 40% sample is shown in Fig. 2a. The measurement precision is about $\pm 10\%$. Both diffusivities become negligible (below our noise level) for $\gamma_0 < 0.8$. They appear to saturate for $\gamma_0 > 2$, though we cannot go higher than 3, where the large displacements make tracking difficult.

Irreversibility occurs only above a well-defined threshold strain amplitude, which depends strongly on the concentration of the suspension. This is shown in Fig. 2b, where we plot the dimensionless reversing diffusivities for three samples at different concentrations as a function of γ_0 . For $\phi = 0.40$, the threshold is close to $\gamma_0 = 0.8$, as can be seen from the linear extrapolation drawn through the circles in Fig. 2b, while for $\phi = 0.20$, the diffusivity becomes measurable only above $\gamma_0 = 3.5$. The strong concentration dependence of the extrapolated threshold is shown in Fig. 3.

These experiments raise a number of interesting questions. For example, what is the role of small imperfections and noise? Brownian motion would contribute displacements of only 10 nm in one period; the particle roughness of 2 nm is much smaller than the particle diameter (220,000 nm). Inertial effects have been shown experimentally to be negligible. Geometrical imperfections could play a role, but cannot explain a threshold.

Assuming that the particle interactions are chaotic and require interactions between at least three particles, as shown by János *et al.*¹¹, a strong concentration dependence of the threshold strain amplitude can be expected, since the probability of multiparticle encounters, and their strength, both depend strongly on concentration. Figure 3 shows that the threshold is roughly proportional to ϕ^{-2} experimentally and that numerical simulations (described later) show similar behaviour, though the data are limited.

Some insight can be obtained by comparing the experimental results to numerical simulations. We adapt the method of stokesian dynamics¹⁹ to simulate the reversing problem. Stokesian dynamics (SD) is akin to molecular dynamics except that the interactions are governed by the low Re or creeping flow equations. For sheared suspensions of neutrally buoyant particles, SD solves the Stokes equations for the fluid subject to the no slip boundary conditions on the surfaces of force-free and torque-free particles, to determine the particle velocities. The many-particle configuration $\mathbf{x}(t)$ evolves in time (neglecting inertia at small Re) according to

$$\frac{d\mathbf{x}}{dt} = \dot{\gamma}(t)\mathbf{U}(\mathbf{x}(t))d \quad (2)$$

where $\dot{\gamma}(t)$ is the instantaneous spatially constant shear rate and $\mathbf{U}(\mathbf{x}(t))$ are the configuration-dependent non-dimensional velocities of the particles. The SD method determines \mathbf{U} for a given distribution

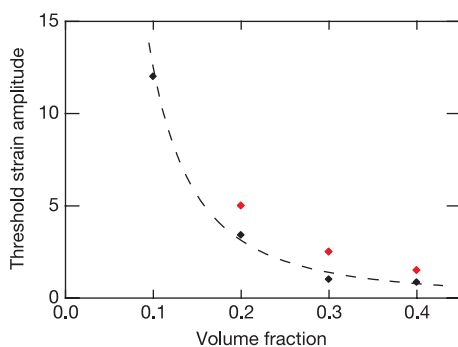


Figure 3 | Threshold strain amplitudes for the onset of irreversibility as a function of volume fraction. Experimental data, black diamonds; numerical simulation, red diamonds; power law fit to data $C\phi^{-\alpha}$, dashed line ($C = 0.14 \pm 0.03$, $\alpha = -1.93 \pm 0.14$). The threshold strain amplitudes are determined from the linear extrapolations in Fig. 2b.

of particles, and then uses equation (2) to evolve the particles in time. At each time step \mathbf{U} is computed anew as the particle configuration changes.

Simulations are performed for $N = 512$ identical spherical particles subject to a bulk shear flow $\mathbf{u} = \dot{\gamma}(t)y\hat{\mathbf{e}}_x$, where $\hat{\mathbf{e}}_x$ is the unit vector in the flow direction and y the spatial coordinate in the velocity gradient direction. Periodic boundary conditions are used in all three directions to minimize boundary effects¹⁹. A square-wave protocol of period T is employed: for $0 < t < T/2$, $\dot{\gamma}(t) = \dot{\gamma}$ and for $T/2 < t < T$, $\dot{\gamma}(t) = -\dot{\gamma}$, which is then repeated. Simulations are performed for total accumulated strains $\gamma = \dot{\gamma}t$ between 400 and 1,000 and for different strain amplitudes $\gamma_0 = \dot{\gamma}T/4$. (The factor of 4 makes the experimental and numerical definitions correspond; the total strain per cycle is $4\gamma_0$ in both cases.)

The positions of all particles are followed in time; their displacements at the end of each period are recorded as a function of total accumulated strain. The mean square displacements exhibit linear growth with total strain at large total strain, just as in the experiments.

As shown in Fig. 4a, the simulations exhibit features similar to the experiments; the effective diffusivities are within a factor of 2–4 of the experiments, agreement that we consider reasonable given that the sources of irreversibility are different in the experiments and simulations. In particular, at small strain amplitudes ($\gamma_0 < 1$) the diffusivities from simulation are very small and of the order of the numerical accuracy of the calculations (which is limited by finite time steps, resolution, and so on). Therefore only qualitative agreement between simulation and experiment is expected.

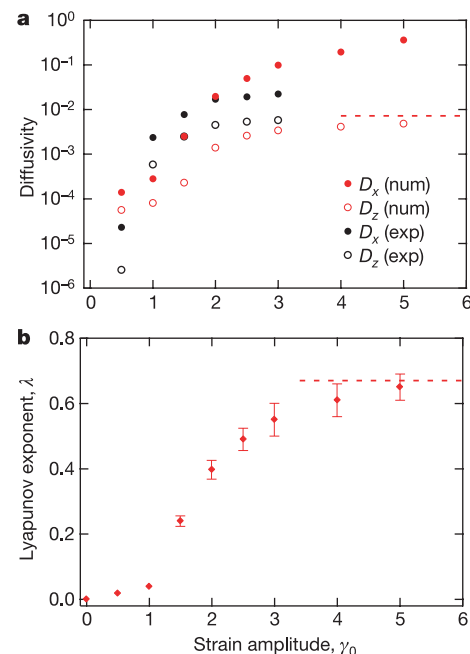


Figure 4 | Diffusivities and Lyapunov exponents. **a**, Numerically computed diffusivities (red symbols; ‘num.’) and experimental diffusivities (black symbols; ‘exp.’) for diffusion in the x (filled circles) and z (open circles) directions as a function of strain amplitude γ_0 for $\phi = 0.40$. In the simulations, the diffusivity D_y (not shown) in the y or velocity-gradient direction is also determined and is found to be intermediate between D_x and D_z . The reversing experiments for D_z at large strain amplitude compare well to steady shear simulations (dashed line), as is expected. **b**, Numerically computed Lyapunov exponent λ versus strain amplitude γ_0 . The rapid growth of λ with increasing γ_0 mirrors the rapid growth of the diffusivity in **a**, and shows that particle trajectories become increasingly sensitive to small perturbations as the strain amplitude increases. The values of λ for the reversing experiments approach the steady state value (dashed line) at large strain amplitude, as is expected. The error bars indicate the standard deviations found from fits to $\delta(t) \sim \exp(\lambda\dot{\gamma}t)$.

The most significant deviation between the simulations and the experiments is for the effective diffusivity at strain amplitudes beyond 2 (recall that the experiments are limited to strain amplitudes below 3 for the most concentrated samples). The experimental diffusivities appear to level off sooner for $\gamma_0 > 2$, which may be due to the finite gap size in the velocity gradient direction ($\sim 11d$) limiting particle excursions; in the simulations, the periodic boundary conditions allow the particles to wander off to infinity in all three directions.

Both the experiments and simulations exhibit a strain amplitude threshold below which the diffusivities drop dramatically. Experimentally, the critical strain amplitude rises from about 1 for $\phi = 0.3$ or 0.4 to more than 10 for $\phi = 0.1$, while in the simulations the threshold is somewhat higher, but still consistent with the ϕ^{-2} scaling mentioned earlier. Some insight concerning the origin of the rapid onset of diffusion with increasing strain amplitude can be gained by examining how rapidly small perturbations are amplified in an oscillating shear flow. To do this, we compute the evolution of two nearby $3N$ particle trajectories and determine their separation $\delta(t)$ in configuration space (spanned by all the $3N$ particle coordinates) following the method of Drazer *et al.*¹⁰. From a pair of SD runs, we find that nearby trajectories separate exponentially in time (or accumulated strain $\gamma = \dot{\gamma}t$) with a positive Lyapunov exponent λ defined by $\delta(t) \sim \exp(\lambda \dot{\gamma}t)$. These simulations reveal a rapid increase in λ with strain amplitude γ_0 , as shown in Fig. 4b, paralleling the behaviour of the diffusivities. The particle trajectories thus become increasingly sensitive to small perturbations as the strain amplitude increases; this supports the conclusion that the chaotic nature of the hydrodynamic interactions between particles leads to the observed irreversible behaviour.

The experiments show that the hydrodynamic interactions can lead to either reversible or irreversible motion, depending on the amount of deformation that is imposed on the suspension. Our numerical results demonstrate that the onset of irreversibility with increasing strain amplitude is associated with the rapid growth of the Lyapunov exponent, which measures the sensitivity of particle trajectories to small perturbations. It is striking that the onset is so marked and that it occurs at relatively small strain amplitudes in concentrated suspensions. Although the creeping flow equations are deterministic, the time (or strain) horizon of predictability is therefore quite limited, extending only out to a total strain of about unity (for concentrated samples). For larger strains, only a statistical description is possible, although important statistical quantities such as the diffusivities can be predicted from numerical solutions to the equations of motion.

These experiments and simulations provide a detailed picture of the onset of irreversibility, the loss of predictability, and the passage from a detailed deterministic description of a many-body dynamical system to a useful statistical description. Whereas some chaotic systems remain reversible for large relative displacements when accurately computed—for example, systems of planets or moons²⁶—suspensions become irreversible and unpredictable after quite small relative displacements. The large number of interacting particles may be responsible.

Received 8 August; accepted 25 October 2005.

1. Tolman, R. C. *The Principles of Statistical Mechanics* (Oxford Univ. Press, London, 1938).
2. Boffeta, G., Cencini, M., Falcioni, M. & Vulpiani, A. Predictability: a way to characterize complexity. *Phys. Rep.* **356**, 367–474 (2002).
3. Wang, G. M., Sevcik, E. M., Mittag, E., Searles, D. J. & Evans, D. J. Experimental

demonstration of violations of the second law of thermodynamics for small systems and short time scales. *Phys. Rev. Lett.* **89**, 050601 (2002).

4. Leal, L. G. *Laminar Flow and Convective Transport Processes: Scaling Principles and Asymptotic Analysis* (Butterworth-Heinemann, Boston, 1992).
5. Morrison, I. D. & Ross, S. *Colloidal Dispersions: Suspensions, Emulsions, and Foams* (Wiley-Interscience, Hoboken, 2003).
6. Lamb, J. S. W. & Roberts, J. A. G. Time-reversal symmetry in dynamical systems: a survey. *Physica D* **112**, 1–39 (1998).
7. Berg, H. C. *Random Walks in Biology* (Princeton Univ. Press, Princeton, New Jersey, 1993).
8. Taylor, G. I. & Friedman, J. *Low Reynolds Number Flows* (National Committee on Fluid Mechanics Films, Encyclopedia Britannica Educational Corp., United States, 1966); available as 'G. I. Taylor and Kinematic Reversibility' in Multi-Media Fluid Mechanics CD-ROM (eds Homsy, G. M.) (Cambridge Univ. Press, Cambridge, 2000).
9. Aref, H. Chaotic advection of fluid particles. *Phil. Trans. R. Soc. Lond. A* **333**, 273–288 (1990).
10. Drazer, D., Koplik, J., Khusid, B. & Acrivos, A. Deterministic and stochastic behaviour of non-Brownian spheres in sheared suspensions. *J. Fluid Mech.* **460**, 307–335 (2002).
11. János, I. M., Tél, T., Wolf, D. E. & Gallas, J. A. C. Chaotic particle dynamics in viscous flows: The three-particle Stokeslet problem. *Phys. Rev. E* **56**, 2858–2866 (1997).
12. Lighthill, J. The recently recognized failure of predictability in Newtonian dynamics. *Proc. R. Soc. Lond. A* **407**, 35–48 (1986).
13. Eckstein, E. C., Bailey, D. G. & Shapiro, A. H. Self-diffusion of particles in shear flow of a suspension. *J. Fluid Mech.* **79**, 191–208 (1977).
14. Leighton, D. & Acrivos, A. Measurement of shear-induced migration of particles in concentrated suspensions. *J. Fluid Mech.* **177**, 109–131 (1987).
15. Breedveld, V., van den Ende, D., Tripathi, A. & Acrivos, A. The measurement of the shear-induced particle and fluid tracer diffusivities by a novel method. *J. Fluid Mech.* **375**, 297–318 (1998).
16. Breedveld, V., van den Ende, D. & Jongschaap, R. Shear-induced diffusion and rheology of noncolloidal suspensions: Time scales and particle displacements. *J. Chem. Phys.* **114**, 5923–5936 (2001).
17. Zarraga, I. E. & Leighton, D. T. Measurement of an unexpectedly large shear-induced self-diffusivity in a dilute suspension of spheres. *Phys. Fluids* **14**, 2194–2201 (2002).
18. Marchioro, M. & Acrivos, A. Shear-induced particle diffusivities from numerical simulations. *J. Fluid Mech.* **443**, 101–128 (2001).
19. Sierou, A. & Brady, J. F. Shear-induced self-diffusion in non-colloidal suspensions. *J. Fluid Mech.* **506**, 285–314 (2004).
20. Segrè, P. N., Herbolzheimer, E. & Chaikin, P. M. Long-range correlations in sedimentation. *Phys. Rev. Lett.* **79**, 2574–2577 (1997).
21. Segrè, P. N., Liu, F., Umbanhowar, P. & Weitz, D. A. An effective gravitational temperature for sedimentation. *Nature* **409**, 594–597 (2001).
22. Voth, G. A. *et al.* Ordered clusters and dynamical states of particles in a vibrated fluid. *Phys. Rev. Lett.* **88**, 234301 (2002).
23. Krishnan, G. P., Beimfohr, S. & Leighton, D. T. Shear-induced radial segregation in bidisperse suspensions. *J. Fluid Mech.* **321**, 371–393 (1996).
24. Crocker, J. C. & Grier, D. G. Methods of digital video microscopy for colloidal studies. *J. Colloid Interf. Sci.* **179**, 298–310 (1996).
25. Taylor, G. I. Dispersion of soluble matter in solvent flowing slowly through a tube. *Proc. R. Soc. Lond. A* **219**, 186–203 (1953).
26. Sussman, G. J. & Wisdom, J. Chaotic evolution of the solar system. *Science* **257**, 56–62 (1992).

Supplementary Information is linked to the online version of the paper at www.nature.com/nature.

Acknowledgements We appreciate discussions with L. G. Leal and G. Homsy. K. Knipmeyer and E. Knowlton provided assistance with data acquisition and reduction. This work was supported by the Keck Foundation (D.J.P.), the National Science Foundation (J.P.G.) and the US-Israel Binational Science Foundation (A.M.L.). The work was initiated during a granular physics workshop hosted by the Kavli Institute for Theoretical Physics at UCSB.

Author Contributions D.J.P. and J.P.G. were responsible for the experiments; J.F.B. and A.M.L. did the numerical simulations.

Author Information Reprints and permissions information is available at npg.nature.com/reprintsandpermissions. The authors declare no competing financial interests. Correspondence and requests for materials should be addressed to D.J.P. (pine@nyu.edu); correspondence concerning the simulations should be addressed to J.F.B. (jfb@cheme.caltech.edu).